

Measurements and comparison of the probability density and covariance functions of laser beam intensity fluctuations in a hot-air turbulence emulator with the maritime atmospheric environment

C. Nelson^{a,b}, S. Avramov-Zamurovic^b, R. Malek-Madani^b, O. Korotkova^c, R. Sova^d, F. Davidson^a

^aThe Johns Hopkins University, 3400 N. Charles Street, Baltimore, MD 21218, USA

^bThe United States Naval Academy, 121 Blake Road, Annapolis, Md 21402, USA

^cThe University of Miami, Coral Gables, FL, 33124, USA

^dThe Johns Hopkins University Applied Physics Laboratory, 11100 Johns Hopkins Road, Laurel, MD 20723, USA;

A hot-air turbulence emulator is employed for generating controlled optical clear air turbulence in the weak fluctuation regime in laboratory conditions. The analysis of the first and second-order statistical moments of the fluctuating intensity of a propagating infra-red (IR) laser beam through the turbulence emulator is made and the results are compared with bi-directional shore-to-ship maritime data collected during a 2009 mid-Atlantic Coast field test utilizing single-mode adaptive optics terminals at a range of 10.7 km, as well as with a 633 nm Helium Neon laser propagating across land and water at the United States Naval Academy.

Keywords: Free-space optical communications, atmospheric turbulence, hot-air turbulence emulator, probability density function, scintillation, maritime

1. INTRODUCTION

A laser beam propagating in a maritime environment can experience significant intensity fluctuations due to optical turbulence along the propagation path, resulting in high bit-error rates (BER) [1]. Working in a controlled laboratory setting that is able to simulate some of the scaled effects of the environment holds great advantages in cost, testing methods, and optimization.

This paper focuses on the first order and second order statistics of the propagating laser beam. Specifically, the single-point probability density function (PDF) and autocovariance function of the propagating laser beam intensity through a hot-air turbulence emulator is compared with field tests conducted by the Johns Hopkins University Applied Physics Laboratory/Johns Hopkins University (APL/JHU) and the United States Naval Academy (USNA). The PDF of the intensity for a given detector is critical for estimation of the fade statistics of an optical signal through the BER and the autocovariance function may be able to provide fundamental insight into the length and depth of the fades through a single exponential fit correlation time.

2. THEORETICAL BACKGROUND

Several PDF models have been suggested and tested for light propagation in random media. We present three models, the Gamma-Laguerre [2],[3], Gamma-Gamma with Aperture Averaging [4, 5] and the Lognormal [6] PDF models in addition to including autocovariance analysis for the different cases.

*cnelson@usna.edu; phone 410-293-6164; fax 443-778-0619; www.usna.edu

A) Gamma-Laguerre PDF model

The approach introduced in [6] and repeated here for clarity is discussed and presented in [3] as the Gamma-Laguerre (GL) PDF model utilizes the Gamma distribution weighted by generalized Laguerre polynomials and has the form:

$$W_{GL}(I) = \frac{1}{\Gamma(\beta)} \left(\frac{\beta}{\mu}\right)^\beta I^{\beta-1} \exp\left(-\frac{\beta I}{\mu}\right) \sum_{n=0}^{\infty} U_n L_n^{(\beta-1)}\left(\frac{\beta I}{\mu}\right), I \geq 0, \quad (1)$$

where, I , is the fluctuating intensity, and $\Gamma(x)$ is the Gamma function and the two parameters of the distribution defined by the first and second moments:

$$\mu = \langle I \rangle, \quad \beta = \langle I \rangle^2 / (\langle I^2 \rangle - \langle I \rangle^2) \quad (2)$$

Additionally, U_n are the weighting coefficients given by:

$$U_n = n! \Gamma(\beta) \sum_{k=0}^n \frac{(-\beta/\mu)^k \langle I^k \rangle}{k!(n-k)! \Gamma(\beta+k)}, \text{ and } U_0 = 1, U_1 = U_2 = 0. \quad (3)$$

The generalized Laguerre Polynomials, $L_n^{(\beta-1)}(x)$ as used in formula (1) are given by:

$$L_n^{(\beta-1)}(x) = \sum_{k=0}^n \binom{n+\beta-1}{n-1} \frac{(-x)^k}{k!} \quad (4)$$

B) Gamma-Gamma Aperture Averaged PDF model

Another model suggested in [4] has become known as the Gamma-Gamma (GG) PDF model. For finite detector sizes, the GG PDF model is modified in [5] to include aperture averaging (GG_A). In contrast to the GL PDF model, the GG and GG_A PDF models require knowledge of a number of atmospheric and source parameters such as propagation distance (L), atmospheric spectrum (for example, the Kolmogorov), and beam radius at launch (W_0). The GG PDF model has the following form:

$$W_{GG}(I) = \frac{2(\alpha\beta_G)^{\frac{\alpha+\beta_G}{2}}}{\Gamma(\alpha)\Gamma(\beta_G)} I^{\frac{\alpha+\beta_G}{2}-1} K_{\alpha-\beta_G}(2\sqrt{\alpha\beta_G I}), I > 0, \quad (5)$$

where $\Gamma(x)$ is the Gamma function as before, $K_m(x)$ is the modified Bessel function of the second kind, I is the normalized intensity, and the parameters α and β_G are defined as follows:

$$\alpha = \frac{1}{\exp(\sigma_{lnx}^2)-1}, \quad \beta_G = \frac{1}{\exp(\sigma_{lny}^2)-1} \quad (6)$$

σ_{lnx}^2 and σ_{lny}^2 are normalized variances of log intensity due to perturbations caused by large and small scales respectively of the turbulent medium. Under the assumption of aperture averaging and the Kolmogorov power spectrum these quantities are given by [8]:

$$\sigma_{lnx}^2 \cong 0.49\sigma_1^2 \left(\frac{\Omega_G-\Lambda_1}{\Omega_G+\Lambda_1}\right)^2 \left(\frac{1}{3} - \frac{1}{2}\overline{\Theta}_1 + \frac{1}{5}\overline{\Theta}_1^2\right) \left[\frac{\eta_x}{1+0.40\eta_x \frac{(2-\overline{\Theta}_1)}{(\Lambda_1+\Omega_G)}}\right]^{\frac{7}{6}}, \text{ and } \sigma_{lny}^2 \cong \frac{1.27\sigma_1^2\eta_y^{-5/6}}{1+\frac{0.40\eta_y}{(\Lambda_1+\Omega_G)}}, \eta_y \gg 1, \quad (7)$$

where

$$\eta_x = \frac{\left(\frac{1}{3} - \frac{1}{2}\bar{\Theta}_1 + \frac{1}{5}\bar{\Theta}_1^2\right)^{-\frac{6}{7}} \left(\frac{\sigma_B}{\sigma_1}\right)^{\frac{12}{7}}}{1 + 0.56\sigma_B^{\frac{12}{5}}}, \quad \eta_y = 3 \left(\frac{\sigma_1}{\sigma_B}\right)^{12/5} (1 + 0.69\sigma_B^{12/5}), \quad (8)$$

$$\Lambda_1 = \frac{\left(\frac{2L}{kW_0^2}\right)}{1 + \left(\frac{2L}{kW_0^2}\right)^2}, \quad \bar{\Theta}_1 = 1 - \Theta, \quad \Theta = [1 + \left(\frac{2L}{kW_0^2}\right)^2]^{-1}, \quad \Omega_G = \frac{16L}{kD^2}, \quad (9)$$

and D is the aperture diameter of the detector, Θ is the refraction parameter in the receiver plane for a collimated beam, W_0 is the initial launch beam radius, L is the propagation distance from the source to receiver, and $k = 2\pi/\lambda$ is the wave number.

$$\sigma_B^2 \cong \sigma_{RGB}^2 \cong 3.86\sigma_1^2 \left\{ 0.40[(1 + 2\Theta)^2 + 4\Lambda_1^2]^{\frac{5}{12}} \cos \left[\frac{5}{6} \tan^{-1} \left(\frac{1+2\Theta}{2\Lambda_1} \right) \right] - \frac{11}{16} \Lambda_1^{5/6} \right\} \quad \text{and} \quad (10)$$

$$\sigma_B^2 = (\langle I^2 \rangle - \langle I \rangle^2) / \langle I \rangle^2 \quad (11)$$

Here, σ_{RGB}^2 , from equation (10), is the Rytov variance for a Gaussian beam wave [5] and is approximated by the scintillation index, σ_B^2 , as measured from the data and given by Eq. (11). Note, this is justified for the weak fluctuation regime where the on-axis variance of the log-irradiance given by $\sigma_{lnI}^2 = var(\ln(I))$, is approximately equal to the scintillation index, or $\sigma_B^2 \cong \sigma_{lnI}^2$ ([5], Secs 1.7 and 5.1). Now, from the measured value of the scintillation index, σ_B^2 , the plane wave Rytov variance, σ_1^2 , from Eq. (10) is computed and applied in Eqns. (7) – (8) for the GG_A Model. From this we compute α and β as given in Eq. (6) and then used in the GG PDF model given by Eq. (5). We label this model the W_{GGA} model.

C) Lognormal PDF model

The Lognormal PDF model is a classic turbulence model and has the following form [6]:

$$W_{LN}(I) = \frac{1}{I\sigma\sqrt{2\pi}} \exp \left[-\frac{[\ln(I) - \mu_{lnI}]^2}{2\sigma^2} \right], \quad I > 0, \quad (12)$$

where μ_{lnI} is the mean and σ_{lnI}^2 is the variance of the log-irradiance.

D) Autocovariance of the log-irradiance

In addition to PDF models for the optical propagation we make comparison of the temporal 2nd order autocovariance function expressed as follows [9]:

$$B_x(t_1, t_2) = \left\langle [x(t_1) - \langle x(t_1) \rangle][x(t_2) - \langle x(t_2) \rangle] \right\rangle \quad (13)$$

For a stationary process the autocovariance function becomes: $B_x(\tau) = R_x(\tau) - m^2$ where $\tau = t_2 - t_1$, $R_x(\tau) = \langle x(t_1)x(t_2) \rangle$ is the correlation function, and m is the mean. For this paper, $x(t_1)$ and $x(t_2)$ represent the log-irradiance values at time t_1 and t_2 respectively.

Through the autocovariance function, the decay constant or typical correlation time of a single exponential fit may give us additional insight and information about the duration and frequency of fades which are so critical for FSO communication systems. The single exponential fit was accomplished through MATLAB's FMINSEARCH function where the general form for the exponential fitting function has the form [10]:

$$B_{(exp\ fit)}(t_{data}) = Ae^{(-t_{data}/T_1)} \quad (14)$$

where T_1 is referred to as the correlation time, or 1/e point for the single exponential.

3. EXPERIMENT DESCRIPTION AND LABORATORY COMPARISON

Figure 1 illustrates the two field test set-ups for comparison.



Figure 1 – (a) JHU/APL 2009 Wallops Island, Va field test [11], (b) Land and creek, USNA.

Additional details on the experiments conducted for the 2009 Atlantic Coast field test, and USNA field tests can be found in [3, 12, 13]. A few highlights of the field tests are presented here. During the Atlantic Coast field tests at Wallops Island, VA, the IR laser beam center was locked in a closed loop onto the 2.54 cm (boat) and 10 cm (Tower) diameter power-in-fiber adaptive optics communication terminals. The power-in-bucket detectors (0.64 and 2.54 cm) were located just off of beam center next to the 2.54 cm power-in-fiber aperture. Field experiments conducted at USNA utilized a 632.8 nm HeNe laser, beam expander, spatial light modulator (SLM) with a constant spatial phase screen and no cycling and which was captured with a high speed (1000 frames/second) digital CCD camera. Data runs were near 3 minutes in length, and the highest average intensity pixel value was determined across all of the captured images. These intensity values were then normalized and used to generate the PDFs directly from moments of the data.

For the case of the 2009 field test data off of the Atlantic Coast, the Histogram, PDF models, and autocovariance functions are presented in this paper at a 10.7 km propagation distance, C_n^2 of approximately $1.5 \cdot 10^{-15} \text{ m}^{-2/3}$ as estimated based on results from reference [12], and as a function of a 0.64 and 2.54 cm power-in-bucket aperture detector, and a 2.54 cm power-in-fiber aperture detector. This collected field test data was then compared with in-laboratory hot-air turbulence emulator results with a similar Fresnel Number and scintillation index for intensity fluctuations of the propagating IR laser beam. Observed realizations are each one minute long, samples of data were collected at 10,000 samples/second or 600,000 data points for the one minute observation time, and then normalized to the mean of the data. The research vessel's average speed through the water was about 2 m/s or 120 meters each minute, giving reasonably constant conditions over the observation time. PDF models from the field test data set represent fluctuating power levels at the

detectors on or near beam center – this condition was achieved through a locked link and detector locations are as described in [14].

The in laboratory hot-air turbulence emulator (see Fig. 2) measures 91.4 cm (3 ft.) in length, and 15.2 cm in height and width (6 inches). The hot-air turbulence emulator is ‘broken’ up into 5 sections of equal distance where the first, second, fourth, and fifth positions are taken up in heat guns and variable speed fans. Ten K-type thermocouple probes were positioned ~3.8 cm apart on either side of the beam propagation path and connected to a data logger that collects temperature readings every 1 second. The heat guns provided thermal flow from one (red arrows in Figure 2a) side while fans provided ambient air counter flow (white arrows in Figure 2a). The air flows met in the middle and created a turbulent propagation channel which was then exhausted through section 3 (both directions). Additionally, three diffuser screens were placed between the heat gun exhaust and the propagation channel where heat gun positioning was done to maximize the temperature difference across the thermocouples.

For the in-laboratory simulation of the field test at USNA a distributed feedback (DFB) laser operating near 1550 nm was connected to a single-mode (SM) fiber, sent to a 1.6 mm diameter fiber collimator, vertically polarized, sent through an IR beam expander, and then reflected from a SLM with window dimensions of 7.68 x 7.68 mm. The SLM was set-up for constant phase modulation across the beam profile with no cycling of the constant phase screen (same as for USNA field test). The beam then passed through a mechanical iris set at 0.6 mm diameter before passing through the hot-air turbulence emulator and on to an InGaAs detector with aperture area of 0.8 mm². The total propagation distance for the USNA simulation was 1.5 m and the mechanical iris was used to match the Fresnel Number, N_f , as computed from [15], with the Wallops Island, VA field test.

For the in-laboratory simulation of the field test off of Wallops Island, Va the set-up was the same as for the USNA simulation with the exceptions that the fiber collimator was propagated directly (no SLM, expander, or polarizer) to the hot-air turbulence emulator for a total propagation distance of 1.9 m. The mechanical iris was not used as the Fresnel Numbers were matched.

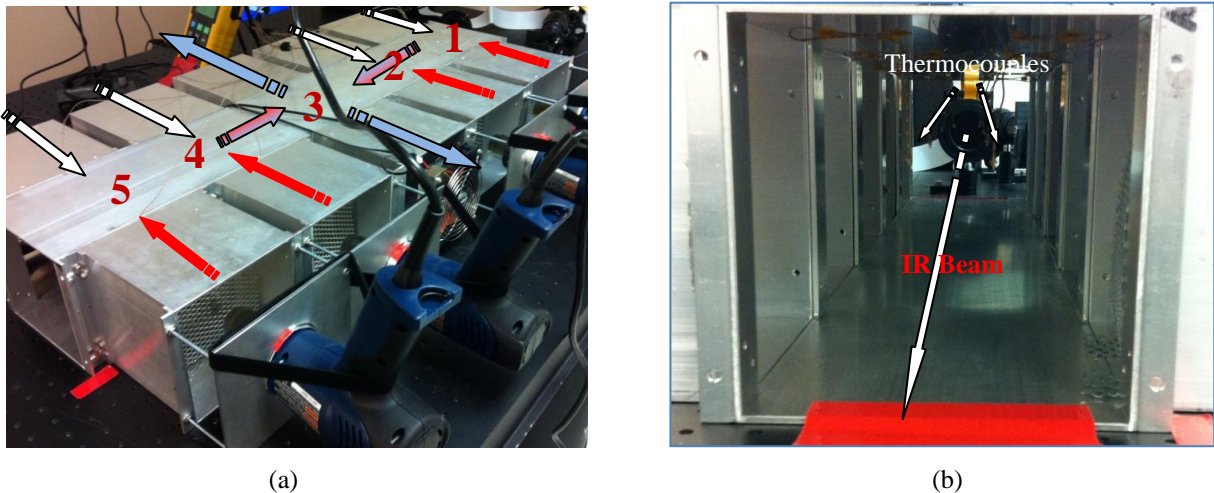


Figure 2 – Hot-air turbulence emulator experimental set-up – (a) air flow in turbulence emulator with sections labeled 1 through 5, (b) propagation channel with thermocouples.

The turbulence in the hot-air turbulence emulator was found to be approximately Kolmogorov along the beam propagation axis as estimated through measurement of the temperature structure

function as a function of thermocouple separation distance through the following equation [9], also known as the Kolmogorov-Obukhov similarity law [16]:

$$D_T(r) = C_T^2 r^{2/3} \text{ for } l_0 \ll r \ll L_0, \quad (15)$$

where the separation distance between thermocouples, r , falls in the inertial subrange defined by the inner scale, l_0 , and outer scale, L_0 , of turbulence.

Figure 3 shows the approximately linear fit over the range of 5 mm to 3.9 cm for the temperature structure function plotted vs. separation distance raised to the (2/3) power. It was found that after 3.9 cm the temperature structure function started to increase faster than the (2/3) linear fit. This effect of an increasing $D_T(r)$ beyond $r^{2/3}$ is in alignment with what Gamo and Majumdar found in their characterization [16]. Additionally, it was found in [16] that a leveling off of the temperature structure function occurred after 7 cm – essentially going constant – this same effect was not seen in our case out to the 8.5 cm maximum distance measured. Gamo and Majumdar explained the effect of a constant temperature structure function as the separation distance exceeding the outer scale of turbulence where the temperature fluctuations between probes is uncorrelated. From this description, we can estimate that the outer scale value in our case was larger than 8.5 cm.

Figure 3 shows a plot of $D_T(r)$ vs. $r^{2/3}$ for the in-lab hot-air turbulence emulator. The slope of the linear fit gives an approximate value of the temperature structure constant, $C_T^2 = 4433 \text{ K}^2/\text{m}^{2/3}$. The heat gun's were set at their lowest setting of 200F and the temperatures were measured at the thermocouples located in section 5 (see Figure 2a and b) of the turbulence emulator.

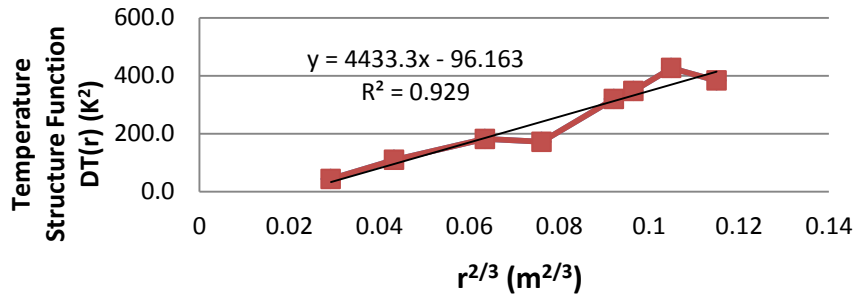


Figure 3 – Plot of Temperature structure function vs. thermocouple separation distance, $r^{2/3}$, for hot-air turbulence emulator.

Note – heat gun settings are not absolute, the heat guns tend to wear out after 70+ hours of use.

The turbulence emulator data was collected at 10,000 samples/second and computed in the same fashion as the data collected during the Wallops Island, Va field test. Additionally, for each run of the hot-air turbulence emulator the refractive index structure parameter, C_n^2 , was approximated utilizing the following equation and method for an IR beam at 1550 nm [9]:

$$C_n^2 = \left(77.8 \times 10^{-6} \frac{P}{T^2} \right) C_T^2, \text{ where } P \text{ is in millibars, } T \text{ is in Kelvin} \quad (16)$$

Specifically, the temperature differences between the ten thermocouples were measured (two for each of the five sections) and from this (ΔT) between thermocouples, the temperature structure function, D_T , was computed and then the temperature structure constant, C_T^2 , from equation (15).

C_T^2 , was then used to estimate C_n^2 for each of the five sections of the hot-air turbulence emulator and then averaged over the ~ 1 meter path length to give an approximate path averaged value. A value of $1 \times 10^{-18} \text{ m}^{-2/3}$ was used to estimate the turbulence strength for the open air propagation sections between source and receiver.

4. RESULTS

The data plots in this section compare the observed scintillation index, σ_B^2 , autocovariance functions through the correlation time, T_I , approximated ratio of the source aperture diameter to spatial coherence radius, D_S/ρ_0 , where ρ_0 , is as computed from [9], the Fresnel Number, N_f , and fade statistics (number of fades, cumulative probability of fade, and channel availability) between field tests performed and the in-laboratory experiments utilizing a hot-air turbulence emulator. The ratio, D_S/ρ_0 , as discussed in a number of papers (see [17] for one example), indicates the scaling of turbulence between atmosphere and laboratory. Additionally, a more detailed analysis of the 1st order PDF analysis of an IR laser beam propagating in a maritime environment can be found in [14] as well as in [3].

The fade statistics were computed by comparing the received intensity with an arbitrary threshold level set at 3 dB below the mean intensity value for the Wallops Island field tests and 1 dB for the USNA data run. Channel availability was computed by taking the number of intensity points above threshold and dividing this by the sum of the points above and below threshold.

Fig. 4 shows a representative figure for the cumulative probability of fade length (2.54 cm power-in-fiber case shown) for the experiments, where Tau is defined as the duration of the fade.

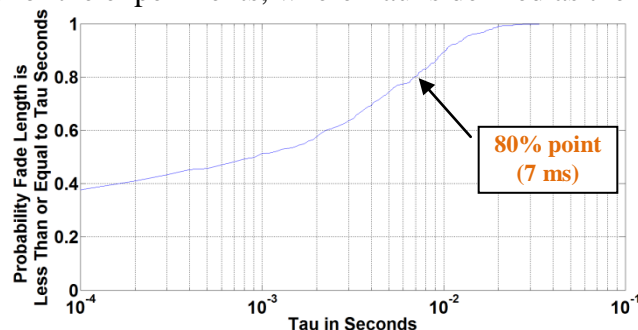


Figure 4 – Cumulative probability of fade for 10.7 km power-in-fiber (reference Fig. 5a) case.

As can be seen in Fig. 5, even though the hot-air turbulence emulator PDF is reasonably close to the other cases, the correlation time is greatly reduced in comparison (1.2 ms vs. 8 – 11 ms). This significant reduction in correlation time, in addition to being the comparison of a closed loop system at sea vs. in-laboratory, could relate the fact that the hot-air turbulence emulator's C_n^2 is approximately 10,000 times stronger over 1 meter as compared to the approximate path averaged atmospheric C_n^2 as measured in [16] and estimated in reference [12] for the 2009 field tests. Also, note that while the number fades (see Table 1) for the emulator is fairly high, 1820, as compared with the 2.54 cm power-in-fiber and 2.54 cm power-in-bucket with 552 and 156 respectively; it is nearly identical to the 0.64 cm power-in-bucket detector.

The comparison of the 80% and 100% times for cumulative probability of channel fades is also notable. The hot-air turbulence emulator had 80% of its fades occurring for about 1 ms or less with the longest fade occurring at 13 ms. This compared to the 2.54 cm power-in-fiber detector's 80% point was at 7 ms, and its 100% point at 34 ms. The 0.64 cm power-in-bucket detector's 80% point was a comparable 1 ms but its 100% point was higher at 31 ms. The 2.54 cm power-in-bucket detector's 80% point was 10 ms and its 100% point was 30 ms, but it had by far the fewest number of fades at 156 which could be attributed to a slightly reduced scintillation index.

While channel availabilities were fairly consistent across the runs it is noted that the 2.54 cm power-in-fiber and 0.64 cm power-in-bucket detector channel availabilities are very close and as shown in Fig. 6, these two detectors have nearly identical PDFs. What can be seen between the two detectors is that there is a near 1 ms difference between the correlation times. This relative difference in correlation time between the two detectors also appears to hold at longer distances (out to near optical horizon at ~17.8 km, data not shown) as well – where the trend is for the overall correlation times to generally reduce as the scintillation and propagation distance increases. Additionally, while the PDF and channel availabilities are near equal, the difference in number of fades between the two detectors is significant 552 vs. 1717. A possible consideration is the ratio of the spatial coherence radius to the detector aperture diameter, ρ_0/D_A . Comparing just the three detectors from the Wallops Island, Va field test data, this ratio is approximately 7 for the 0.64 cm power-in-bucket detector, and 2 for the 2.54 cm power-in-fiber and power-in-bucket cases. For example, comparing the 0.64 cm and the 2.54 cm power-in-bucket and power-in-fiber it could be that the higher ratio drives a higher number of fades, shorter correlation times, and shorter overall fade lengths.

Case	Approx. $\frac{D_s}{\rho_0}$	σ_B^2	N_f	Corr. time, T_I (ms)	Number of Fades	80% and 100% Cum. Prob. of fade times (ms)	Channel Avail.
2.54 cm power-in-fiber, Wallops Island, VA (Fig. 5a)	2	0.123	0.15	9.54	552	7 and 34	96.7%
0.64 cm power-in-bucket Wallops Island, VA (Fig. 5b)	2	0.129	0.15	8.68	1717	1 and 31	96.4%
2.54 cm power-in-bucket, Wallops Island, VA (Fig. 5c)	2	0.097	0.15	11.24	156	11 and 30	98.2%
In-laboratory hot-air turbulence emulator (Fig. 5d)	1	0.128	0.22	1.2	1820	1 and 13	97.1%

Table 1 – summary of Wallops Island field test data and comparison with turbulence emulator

So, the PDF, scintillation index, and channel availability in the hot-air turbulence emulator are comparable to the field tests while the number of fades is relatively high (especially as compared with the 2.54 cm power-in-bucket and power-in-fiber), but the overall duration of the fades (1 to 13 ms) appears reduced in comparison. This leads to the possible conclusion that while 1st order statistics are vital, the 2nd order statistics of intensity could give valuable insight into the length and number of fades for the channel. Specifically, the greatly reduced correlation time for the hot-air turbulence emulator appears to reduce the general probability of a longer length fade. This may also be seen for the 0.64 cm power-in-bucket detector which also had a high number of fades, but a shorter correlation time and also a generally reduced 80% and 100% cumulative probability of fade.

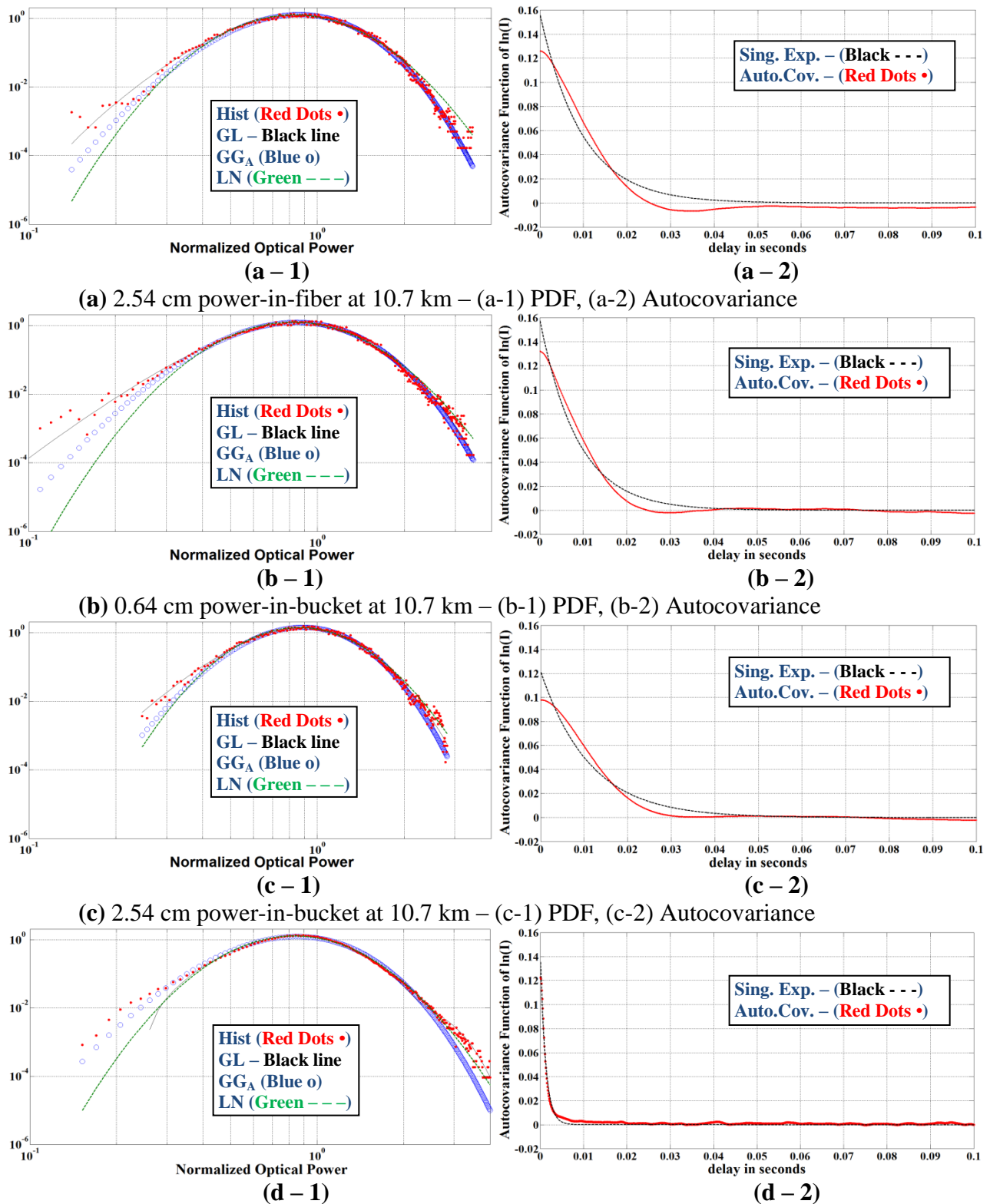


Figure 5 – Comparison of Turbulence emulator with IR laser beam in the maritime environment.

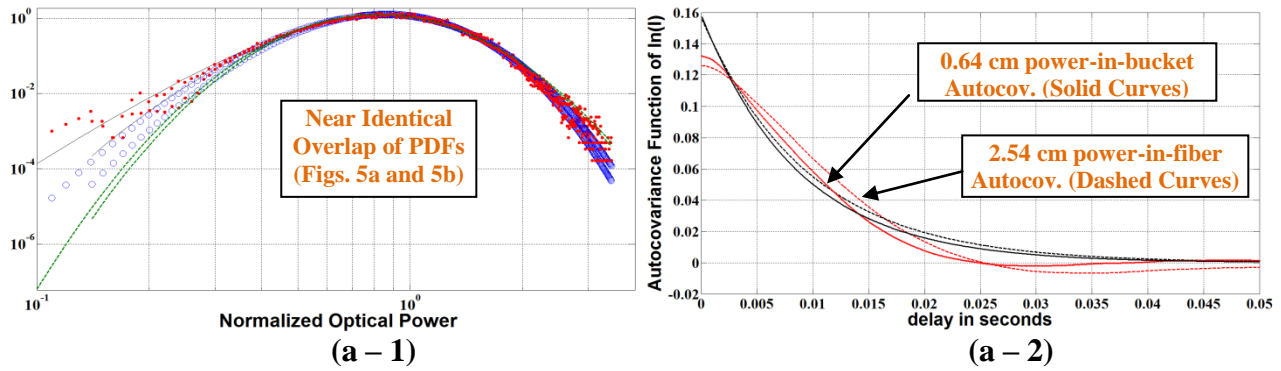


Figure 6 – Overlap of 2.54 cm power-in-fiber and 0.64 cm power-in-bucket detectors (Figs. 5a and 5b) – (a-1) PDF, (a-2) Autocovariance

For the case of the land and creek field test at USNA (see Fig. 7), only the GL and LN PDFs are shown due to lower scintillation and inability to adequately fit the GG PDF. Additionally, since the data was captured at 1000 samples per second for the CCD camera, the turbulence emulator data was averaged over every 10 samples to achieve an effective 1000 samples/second from the 10,000 samples second that were collected. As summarized in Table 2, the correlation time for the land and creek USNA data set was very low, 0.3 ms. The explanation for the difference between this and the data collected at Wallops Island, Va (9 to 11 ms) is not clear, but partly could relate the use of the closed loop adaptive optics. Additionally, as discussed previously, there appears to be a possible relationship between the correlation time, and the ρ_0/D_A ratio to the relative number and duration of fades. Specifically, for the USNA field test, the CCD camera’s ρ_0/D_A ratio was very high owing to the fact that the intensity was captured on a single pixel as compared to a spatial coherence radius on the order of 8 cm. This greater ρ_0/D_A ratio as well as low correlation time (0.3 ms compared with 1.5 ms) could indicate a generally higher number of fades (3384 compared with 2092) as well as a reduced duration of the longer fades (all essentially at 1 ms, or single point fades). As discussed, this was also seen with the 0.64 cm power-in-bucket detector (from Table 1) when compared with the other two detectors during the Wallops Island, Va field test. Additional differences for this data set could include wavelength differences (632.8 nm HeNe vs. near 1550 nm) as well as differences in the detector types (CCD camera vs. InGaAs detector).

Case	Approx. $\frac{D_s}{\rho_0}$	σ_B^2	N_f	Corr. time (ms)	No. of Fades	80% and 100% cum. Prob. of fade times (ms)	Channel Avail.
Overland and water, 650 m (Fig. 7a)	0.1	0.0137	0.04	0.3	3384	All essentially at 1 ms data capture rate (single point fades)	96.5%
In-laboratory hot-air turbulence emulator (Fig. 7b)	0.1	0.0141	0.04	1.5	2092	1 to 6	96.7%

Table 2 – summary of 650 m land and creek data at USNA and comparison with emulator

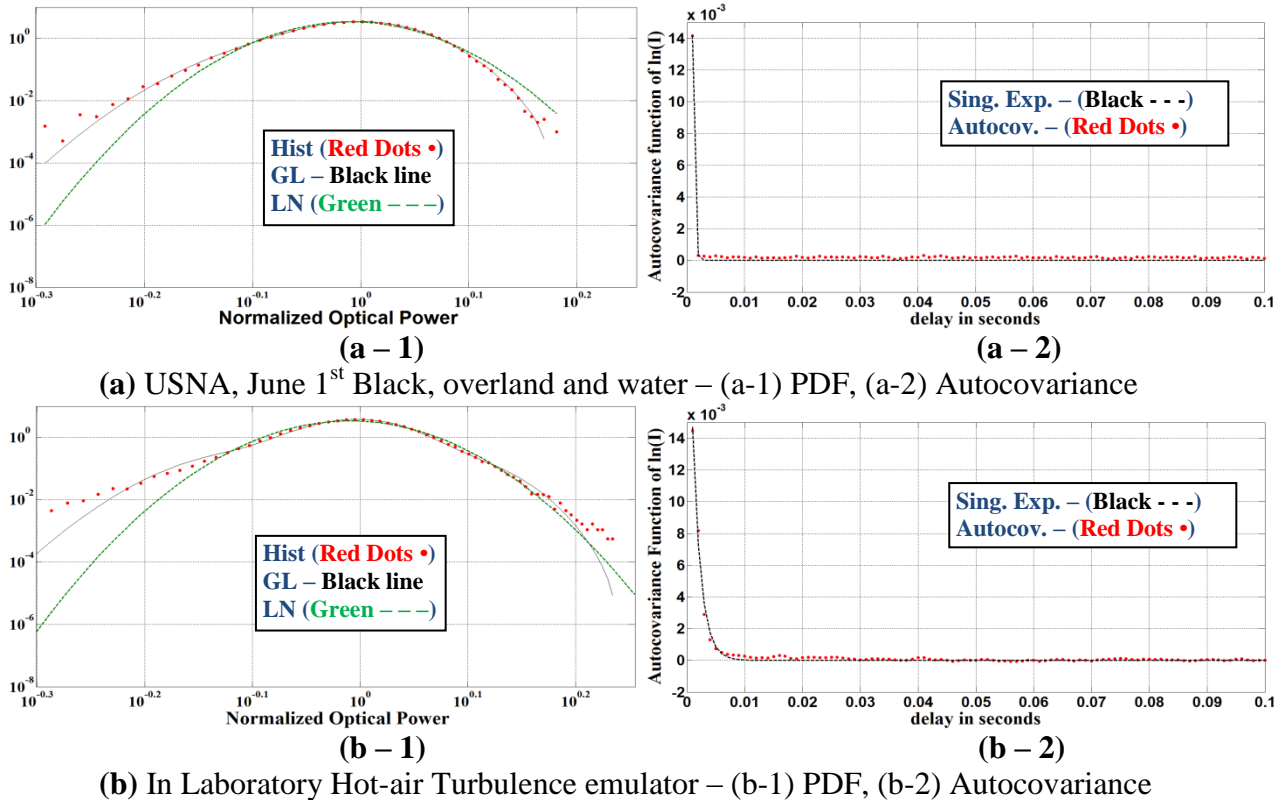


Figure 7 – Comparison of Turbulence emulator with IR laser beam in the maritime environment as well as visible laser beam over land and creek.

5. CONCLUSIONS

In summary, the 1st and 2nd order statistics through the single-point PDF and temporal autocovariance function of the intensity of a laser beam propagating in the maritime environment was compared with a laser beam propagated through an in-laboratory hot-air turbulence emulator. It was shown that the hot-air turbulence emulator could closely match the scintillation index of the field test data with a corresponding closeness of the PDF. It was also shown that even with similar PDFs, the 2nd order autocovariance correlation times differed. From analysis of the fade statistics, it was speculated that the correlation time, as well as ratio of the spatial coherence radius to the detector size may provide increased insight into the overall number and duration of fades in the propagating laser beam.

6. REFERENCES

- [1] Mayer, K. J., Young, C. Y., "Effect of atmospheric spectrum models on scintillation in moderate turbulence," *J. Mod. Opt.* **55**, 1362-3044 (2008)
- [2] Barakat, R., "First-order intensity and log-intensity probability density functions of light scattered by the turbulent atmosphere in terms of lower-order moments," *J. Opt. Soc. Am.* **16**, 2269 (1999)
- [3] Korotkova, O., Avramov-Zamurovic, S., Malek-Madani, R., and Nelson, C., "Probability density function of the intensity of a laser beam propagating in the maritime environment," *Optics Express*. Vol. 19, No. 21, (2011)
- [4] Al-Habash, M. A., Andrews, L. C., and Phillips, R. L., "Mathematical model for the irradiance probability density function of a laser beam propagating through turbulent media," *Opt. Eng.* **40**, 1554-1562 (2001)
- [5] Andrews, L. C., Phillips, R. L., and Hopen, C. Y., [*Laser Beam Scintillation with Applications*], SPIE Press, Bellingham, WA, (2001).
- [6] Aitchison, J. and Brown, J. A. C., [*The Lognormal Distribution*], Cambridge University Press, (1957)
- [7] Lyke, S. D., Voelz, D. G., and Roggemann, M. C., "Probability density of aperture-averaged irradiance fluctuations for long range free space optical communication links," *Applied Optics* Vol. 48, No. 33, (2009)
- [8] Wayne, D. T., Phillips, R. L., Andrews, L. C., Leclerc, T., Sauer, P., Stryjewski, J., "Comparing the Log-Normal and Gamma-Gamma Model to Experimental Probability Density Functions of Aperture Averaging Data," *Proc. SPIE* 7814, (2010)
- [9] Andrews, L. C., and Phillips, R. L., [*Laser Beam Propagation through Random Media*, ^{2nd} edition], SPIE Press, Bellingham, WA, (2005).
- [10] Pratap, R., [*Getting Started with MATLAB 7, a Quick Introduction for Scientists and Engineers*], Oxford University Press, (2006).
- [11] Juarez, J. C., Sluz, J. E., Nelson, C., Airola, M. B., Fitch, M. J., Young, D. W., Terry, D., Davidson, F. M., Rottier, J. R., and Sova, R. M., "Free-space optical channel characterization in the maritime environment," *SPIE Conference presentation*, (2010)
- [12] J.C. Juarez, J. E. Sluz, C. Nelson, M. B. Airola, M. J. Fitch, D. W. Young, D. Terry, F. M. Davidson, J. R. Rottier, and R. M. Sova, "Free-space optical channel characterization in the maritime environment," *Proc. SPIE* 7685, (2010)
- [13] Korotkova, O., Avramov-Zamurovic, S., Nelson, C., Malek-Madani, R., "Probability density function of partially coherent beams propagating in the atmospheric turbulence," *Proc. SPIE* 8238, (2012)
- [14] Nelson, C., Avramov-Zamurovic, S., Korotkova, O., Malek-Madani, R., Sova, R., Davidson, F., "Probability density function computations for power-in-bucket and power-in-fiber measurements of an infrared laser beam propagating in the maritime environment," *Proc. SPIE* 8038, (2011)
- [15] Goodman, J. W., [*Introduction to Fourier Optics*, ^{2nd} edition], McGraw-Hill Co. Inc., (1996).
- [16] Gamo, H., and Majumdar, A., "Atmospheric turbulence chamber for optical transmission experiment: characterization by thermal method," *Applied Optics* Vol. 17, No. 23, 3755-3762 (1978)
- [17] Phillips, J. D., "Atmospheric Turbulence Simulation Using Liquid Crystal Spatial Light Modulators," Air Force Institute of Technology Masters Thesis, (2005)